Translational Cancer Mechanisms and Therapy

Clinical Cancer Research

Patient-Derived Cancer Organoid Cultures to Predict Sensitivity to Chemotherapy and Radiation

Cheri A. Pasch[1], Peter F. Favreau[2], Alexander E. Yueh[3], Christopher P. Babiarz[3], Amani A. Gillette[4], Joe T. Sharick[2], Mohammad Rezaul Karim[2], Kwangok P. Nickel[1,5], Alyssa K. DeZeeuw[3], Carley M. Sprackling[1], Philip B. Emmerich[3], Rebecca A. DeStefanis[3], Rosabella T. Pitera[3], Susan N. Payne[1], Demetra P. Korkos[3], Linda Clipson[6], Christine M. Walsh[2], Devon Miller[3], Evie H. Carchman[1,7], Mark E. Burkard[1,3], Kayla K. Lemmon[1], Kristina A. Matkowskyj[1,8,9], Michael A. Newton[10], Irene M. Ong[1,10], Michael F. Bassetti[1,5], Randall J. Kimple[1,5], Melissa C. Skala[1,2,4], and Dustin A. Deming[1,3,6]

Abstract

Purpose: Cancer treatment is limited by inaccurate predictors of patient-specific therapeutic response. Therefore, some patients are exposed to unnecessary side effects and delays in starting effective therapy. A clinical tool that predicts treatment sensitivity for individual patients is needed.

Experimental Design: Patient-derived cancer organoids were derived across multiple histologies. The histologic characteristics, mutation profile, clonal structure, and response to chemotherapy and radiation were assessed using bright-field and optical metabolic imaging on spheroid and single-cell levels, respectively.

Results: We demonstrate that patient-derived cancer organoids represent the cancers from which they were derived, including key histologic and molecular features. These cultures were generated from numerous cancers, various biopsy sample types, and in different clinical settings. Next-generation sequencing reveals the presence of subclonal populations within the organoid cultures. These cultures allow for the detection of clonal heterogeneity with a greater sensitivity than bulk tumor sequencing. Optical metabolic imaging of these organoids provides cell-level quantification of treatment response and tumor heterogeneity allowing for resolution of therapeutic differences between patient samples. Using this technology, we prospectively predict treatment response for a patient with metastatic colorectal cancer.

Conclusions: These studies add to the literature demonstrating feasibility to grow clinical patient-derived organotypic cultures for treatment effectiveness testing. Together, these culture methods and response assessment techniques hold great promise to predict treatment sensitivity for patients with cancer undergoing chemotherapy and/or radiation.

Introduction

A major limitation in clinical oncology is the lack of a reliable method to predict treatment response. Precision medicine is an emerging therapeutic approach that uses the molecular profile of cancers to guide therapeutic choices for patients. This approach has led to significant successes (1–4). Unfortunately, even when molecular targets are present, many cancers are intrinsically resistant to precision medicine strategies, or resistance emerges quickly. The process of matching therapies to an individual patient's cancer is based on many assumptions, and unfortunately, often fails (5). Cancer hotspot sequencing alone is not sufficient to predict response to targeted therapies or standard-of-care chemotherapy and radiation techniques. The development of a robust method to predict the sensitivity of a patient's cancer therapies would be a major advance.

Improved methods to predict the benefit of standard and novel therapies are needed to advance treatment options for patients with cancer. This would prevent unnecessary side effects and decrease the time required to identify an effective treatment strategy. A major limitation in the development of strategies to predict treatment sensitivity has been the inability to reliably culture patient-derived tissues in an inexpensive and

[1]University of Wisconsin Carbone Cancer Center, Madison, Wisconsin. [2]Morgridge Institute for Research, Madison, Wisconsin. [3]Division of Hematology and Oncology, Department of Medicine, University of Wisconsin–Madison, Madison, Wisconsin. [4]Department of Biomedical Engineering, University of Wisconsin–Madison, Madison, Wisconsin. [5]Department of Human Oncology, University of Wisconsin–Madison, Madison, Wisconsin. [6]McArdle Laboratory for Cancer Research, Department of Oncology, University of Wisconsin–Madison, Madison, Wisconsin. [7]Department of Surgery, University of Wisconsin–Madison, Madison, Wisconsin. [8]Department of Pathology and Laboratory Medicine, University of Wisconsin–Madison, Madison, Wisconsin. [9]William S. Middleton Memorial Veterans Hospital, Madison, Wisconsin. [10]Departments of Statistics and of Biostatistics and Medical Informatics, University of Wisconsin–Madison, Madison, Wisconsin.

Note: Supplementary data for this article are available at Clinical Cancer Research Online (http://clincancerres.aacrjournals.org/).

Corresponding Author: Dustin A. Deming, University of Wisconsin-Madison, 1111 Highland Ave, Madison, WI 53705. Phone: 608-265-1042; Fax: 608-265-8133; E-mail: ddeming@medicine.wisc.edu

Clin Cancer Res 2019;25:5376–87

doi: 10.1158/1078-0432.CCR-18-3590

Translational Relevance

The lack of predictive biomarkers is a major limitation in clinical oncology. Patient-derived cancer organoids are a major advance as they are readily generated and represent the tumors from which they are derived. This study further demonstrates the ability of these cultures to represent the phenotypic and molecular heterogeneity within cancers. In addition, this study establishes therapeutic thresholds for further validation using changes in organoid growth rate and optical metabolic imaging. These techniques measure organoid-level and single-cell level therapeutic heterogeneity, respectively. Here these techniques are applied for determining differential response of colorectal cancers to chemotherapy and radiation. In addition, this is one of the first studies to prospectively examine the use these cultures to predict response for an individual patient with cancer.

high-throughput methodology. Prior techniques used to develop sensitivity platforms have relied on nongrowing patient specimens, such as tumor sections on slides or pelleted cancer cells (6–8). There is significant concern that these models do not reliably represent the cancers from which they were derived, and none of these platforms are recommended for standard-of-care use (9). Patient-derived xenograft methods have become an important preclinical tool, but owing to their immense cost and inherent low-throughput nature, this technology has not been adapted in a clinically meaningful way for real-time sensitivity testing (10).

Patient-derived cancer organoids (PDCOs) allow for cancer cells to be grown in a three-dimensional matrix and have been a major advance in the ability to grow cancer cells from patients in a manner that is both timely and cost-effective for clinical impact (11–17). A critical step toward widespread adoption of PDCOs is establishing the feasibility of using these cultures to screen therapeutics for individual patients with cancer. Feasibility is not established based on one investigation, but established over time with studies confirming key findings and adding additional experience and data to the field. Prior studies, using largely small cohorts of PDCOs, have demonstrated that these cultures are reliably generated often with very complex culture media, represent the tumors from which they were derived using phenotypic and molecular analyses, and preliminary retrospective data indicating that the response in PDCOs might predict response in patients (11–17).

Further analyses are needed to examine phenotypic and molecular heterogeneity within these cultures and to determine the ability of these cultures to demonstrate heterogeneity in response. In addition, more simplified culture conditions would allow for these cultures to be more readily available to other investigators. Prior studies have not examined the use of PDCOs to determine differential sensitivity to chemotherapy and radiation for colorectal cancer and have not examined predicting treatment response prospectively. Our laboratory has cultured patient-derived specimens from a variety of cancer types with a primary focus on cancers of the gastrointestinal tract from a variety of types of specimens and using simplified culture media. A label-free assessment technique, optical metabolic imaging (OMI), is used to further quantify cell-level patient response to treatment in organoids (16–18). Here we present the results from culturing over 90 patient-derived specimens and the potential utility of this technology for predicting patient response to chemotherapy and radiation.

Materials and Methods

Cell isolation and organoid culture

All studies involving human tissue were performed with approval from the University of Wisconsin–Madison Institutional Review Board with informed consent obtained from patients and in accordance with the Declaration of Helsinki. Spheroids were isolated and cultured following protocols reported previously (19) with a few modifications (see Supplementary Methods). Human tissue from needle biopsy or surgical resection was placed in chelation buffer and then digested in advanced DMEM/F12 medium (Invitrogen) containing FBS, collagenase, dispase, and antibiotics. The tissues were disrupted with intermittent shaking. Culture medium components were dependent on tissue type (Supplementary Tables S1 and S2). Cell suspensions were maintained on ice and mixed with Matrigel at a 1:1 ratio before being plated as droplets onto multi-well culture plates and incubated at 37°C. Plates were inverted after two to three minutes of incubation. After the mixture had solidified, cultures were overlaid with feeding medium.

Pharmacologic agents

5-fluorouracil (5-FU) and oxaliplatin were obtained from the University of Wisconsin Carbone Cancer Center Pharmacy.

Organoid chemoradiation *in vitro* studies

Organoids were plated in 24-well culture plates and allowed to grow for 1–7 days. Images were taken on a Nikon Ti-S inverted microscope using a 4× objective prior to chemoradiation treatment. After imaging, feeding medium was replaced with feeding medium containing 5-FU at the desired concentrations and spheroids were subsequently exposed to ionizing radiation using a JL-Shepherd ^{137}Cesium Irradiator delivering a dose rate of approximately 400 cGy/minute or an Xstrahl RS-225 cabinet delivering a dose rate of approximately 3.27 Gy/minute. After 2 days, the culture medium was replaced with standard feeding medium. Posttreatment images were obtained on day 4. The images were analyzed using ImageJ. All experiments were completed in triplicate.

Multiphoton imaging *in vitro* studies

Multiphoton imaging was performed as described previously (16, 17). Briefly, NAD(P)H and FAD were excited at 750 nm and 890 nm, respectively, using a tunable Ti:sapphire laser (Coherent, Inc). NAD(P)H emission was isolated from 400 to 480 nm, and FAD emission was isolated from 500 to 600 nm using customized filter cubes. Fluorescence images were acquired using time-correlated single-photon counting (Becker & Hickl SPC-150) over 60 seconds with a pixel dwell time of 4.8 μs. Excitation and emission light were coupled in a 40× water immersion objective (Nikon, 1.15 NA). Emission was detected using a GaAsP photomultiplier tube (H7422P-40, Hamamatsu Photonics). Spheroid imaging occurred 4 days after treatment, with a minimum of three fields-of-view acquired per day per sample (six images total to obtain single-cell analysis of 350–1,000 cells per treatment type).

Image analysis

NAD(P)H and FAD images were created by integrating all detected photons for each pixel per image. Fluorescence lifetimes were extracted using SPCImage software (SPCImage, version 4.8, Becker & Hickl GmbH). Fluorescence lifetimes were fit to a biexponential curve using

$$I(t) = \alpha_1 exp\left(-\frac{t}{\tau_1}\right) + \alpha_2 exp\left(-\frac{t}{\tau_2}\right) + C$$

where $I(t)$ is the fluorescence intensity at time t, α_1 and α_2 are the fractional components of free or bound states of either NAD(P)H or FAD, τ_1 and τ_2 are the short and long lifetime components, and C accounts for background light. The mean fluorescence lifetime was calculated using

$$\tau_m = \alpha_1\tau_1 + \alpha_2\tau_2$$

The optical redox ratio was calculated by dividing NAD(P)H fluorescence intensity by the FAD fluorescence intensity for each pixel. A semiautomated cell segmentation algorithm was developed using Cell Profiler software and performed on NAD(P)H and FAD images to measure the fluorescence intensity in the cytoplasm of each cell in a spheroid, as described previously (18). All pixels were averaged within a cell cytoplasm to calculate one redox ratio per cell.

The collective cell population of each treatment type was input into a Gaussian mixture distribution model (MATLAB, version 2014a, MathWorks) given by (20)

$$f(y;\Phi_g) = \sum_{i=1}^{g} \pi_i \phi(y;\mu_i, V_i)$$

where g is the number of subpopulations, $\phi(y;\mu_i, V_i)$ is the normal probability density function with mean μ_i, variance V_i, and π_i is the mixing proportion. Goodness of fit was calculated given a set of subpopulations ($g = 1$, 2, or 3) using an Akaike information criterion (21). The number of subpopulations was determined on the basis of the lowest Akaike score. Probability density functions were normalized to ensure that the area under the curve for each treatment group was equal to 1. Treatment effect size was calculated using Glass delta (22).

Histologic processing and staining

Organoids were fixed in 2% paraformaldehyde for 15 minutes. Hematoxylin and eosin (H&E) staining was performed as described previously (19).

Results

PDCOs can be generated across diverse clinical specimens

PDCOs were generated across a diverse collection of organ types and histologies, including colorectal, pancreatic, and lung adenocarcinomas, neuroendocrine tumors from several organs, as well as other tumors as shown in Fig. 1 and Supplementary Table S1. Media conditions varied depending on the tumor histology (Supplementary Table S2). The overall rate of spheroid formation was 78% (Supplementary Table S1). Specifically, for colorectal cancer (Supplementary Table S3), pancreatic adenocarcinoma (PDAC), and neuroendocrine tumors (NET), the rates were 76%, 79%, and 90%, respectively. Treatment studies are typically able to be performed within 1 week of culturing with spheres requiring passaging every 1–4 weeks. Many of these cultures were able to be passaged multiple times. Of those samples where multiple passages were attempted, 49% were successfully passaged at least twice.

PDCOs were generated from diverse patient samples obtained through a variety of collection methods, including surgical specimens, core needle biopsies, and malignant fluid samples (paracentesis). Similar success rates were seen across the various sample collection methods (Supplementary Table S1). In addition, similar spheroid formation rates were observed regardless of whether the patient had received prior chemotherapy or radiation (Supplementary Table S1). Common reasons why some samples did not form spheres or were not able to be successfully passaged include paucicellular specimens, necrotic samples, or fungal contamination. It should be noted that this data is inclusive of all our samples, including those obtained when optimizing the technique and media conditions.

Organoids retain key phenotypic characteristics of the tumors from which they were derived

Hematoxylin and eosin (H&E) staining of whole mounts of the resulting PDCOs were compared with H&E-stained sections from corresponding formalin-fixed, paraffin-embedded sections of the original patient tumor. In all instances, the spheroid cultures were similar to the tumors from which they were derived. Corresponding features include secondary architecture, nuclear pleomorphism, nuclear to cytoplasmic ratio, presence of prominent nucleoli, and mitotic rate (Fig. 1A). The colorectal cancer spheroids commonly developed crypt-like structures reminiscent of the malignant glands seen within the patient's cancer (Fig. 1A and C). In addition, organoids derived from mucinous adenocarcinomas were found to produce mucin (Fig. 1D). These key phenotypic characteristics are maintained across passages as long as the culture conditions are maintained.

Key molecular characteristics of the tumors are retained in PDCOs

Prior studies have examined the molecular differences in small cohorts of organotypic cultures and their parent tumors. These studies have largely used DNA copy-number analyses and low-depth sequencing platforms to demonstrate the maintenance of molecular features between the tumor and spheroids (23–25). We performed high-depth targeted cancer gene sequencing using the Qiagen Comprehensive Cancer Panel (275 genes) and molecular barcode technology. Matched low-passage spheroid cultures (range, 1–6 passages) and adjacent tumor tissue were sequenced for seven patients with greater than 500× median coverage across the interrogated genes. Overall, the PDCOs were highly representative of the corresponding tumors (Fig. 2). For the mismatch repair–proficient cancers, 97% of the nonsynonymous mutations were shared between the patient's cancer and the resulting PDCOs (Fig. 2A, far right). One patient's cancer possessed mismatch repair deficiency secondary to a truncating mutation in MSH2; only 40% of the nonsynonymous mutations were shared between the PDCOs and the adjacent tumor (Fig. 2A, sample DC46).

Mutations known to enhance the selective growth advantage of the cancer cells, or driver mutations, were specifically examined. Those driver mutations identified within the primary tumor were overwhelmingly present in the PDCOs. Interestingly, there were instances of incomplete overlap in the driver mutations present. In DC47, a subclonal mutation in *PIK3CA* (E545K, allele frequency of 19%) was identified within the PDCOs, but not the

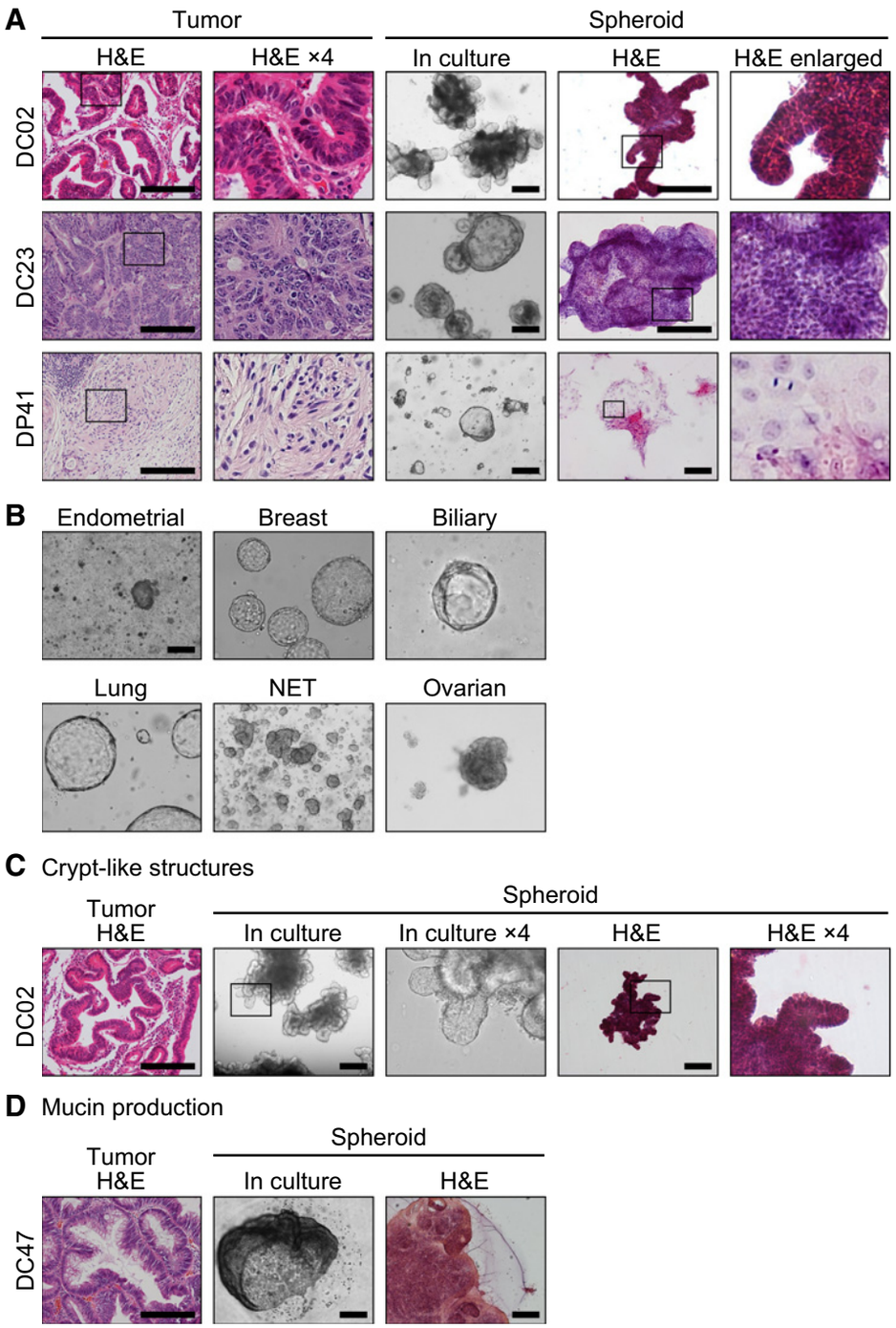

Figure 1.

PDCOs were generated across multiple cancer types and phenotypically represent the tumors from which they were derived. **A,** H&E-stained tumor sections and whole mounts of PDCOs generated from the tissue that was adjacent to that shown in the tumor section (DC, colorectal cancer; DP, pancreatic adenocarcinoma). These PDCOs demonstrate similar secondary architecture, nuclear pleomorphism, nuclear-to-cytoplasmic ratio, presence of prominent nucleoli and mitotic rate. **B,** Brightfield images of PDCOs generated from multiple histologic types of cancer. **C,** Colorectal cancer PDCOs develop crypt-like structures reminiscent of malignant glands within the tumor. **D,** PDCOs generated from mucinous adenocarcinomas also produce mucin. Tumor H&Es are all at the same magnification; scale bars, 100 μm. Spheroids in culture are all at the same magnification; scale bars, 500 μm. Spheroid H&E scale bars, 200 μm. Outlined areas are enlarged in panels to the right.

adjacent tumor. Truncating mutations in *APC* were identified in both the tumor and PDCOs from the mismatch repair–deficient cancer (DC46), but these were not completely identical alterations (E268* and S1861Y in the tumor; E268*, S1861Y, R1114*, and R2237* in the PDCOs). Also, an additional *KRAS* alteration (A147T, allele frequency of 13%) was found in the mismatch repair–deficient organoids that was not present in the tumor sample.

We next sought to identify whether subclonal populations could be resolved by examining molecular heterogeneity within the PDCOs. First, we examined the allele frequency of mutations in well-defined driver genes (Fig. 2B) to determine the cellular purity of these samples. In the four samples queried, oncogenes were mutated with an allele frequency of at least 50% and tumor suppressor alterations with an allele frequency of 100%, indicating that these cultures were a nearly pure

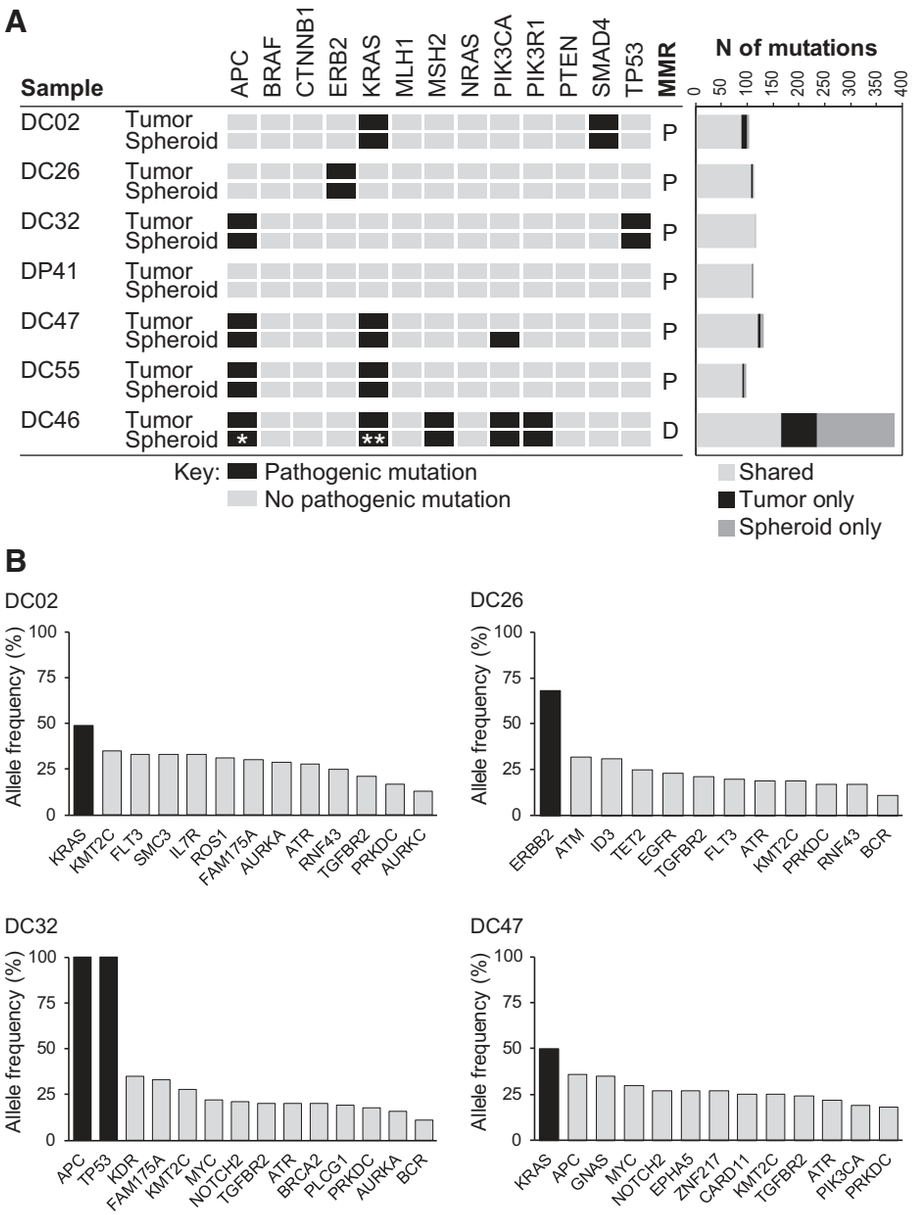

Figure 2.

Cancer hotspot next-generation sequencing was performed comparing each patient's bulk tumor sample and the associated PDCOs (DC, colorectal cancer; DP, pancreatic adenocarcinoma). **A,** The nonsynonymous mutations were similar between the tumor and PDCOs for the microsatellite-stable cancers (MMR, mismatch repair; P, proficient; D, deficient). DC46 is a mismatch repair–deficient tumor, and in this case, an increased number of nonsynonymous mutations were identified as unique to the PDCOs or the adjacent tumor sample. In addition, alterations in known driver genes were identical between the PDCOs and the adjacent cancer except for DC47 in which a subclonal *PIK3CA* E545K mutation was found unique to the PDCOs and the mismatch repair–deficient DC46 cancer that had additional alterations in *APC* (*) and *KRAS* (**) that were not found in the bulk tumor sample. **B,** To examine the prevalence of subclonal populations with the PDCOs, first the allele frequency of known alterations was examined. The allele frequencies were approximately 50% for the founder driver oncogenes and 100% for founding tumor suppressor genes across the samples queried (black bars). For each sample, those alterations with an allele frequency of 10%–35% were identified (gray bars); these indicate the presence of subclonal populations within the PDCOs. Spheroid passage (p) numbers at the time of sequencing are: DC02 p6, DC26 p2, DC32 p4, DP41 p1,DC46 p1, DC55 p1, and DC46 p6.

population of cancer cells as expected (Fig. 2B, black bars). The presence of nonsynonymous mutations with allele frequencies between 10% and 35% were identified as indicative of subclonal populations. Prior investigations have used this allele frequency range to denote subpopulations of cancer cells (26). For each sample, multiple alterations were identified with allele frequencies within this range (Fig. 2B, gray bars). While technical sequencing artifacts can result in identification of some low-level alterations, the number and prevalence of these alterations make the presence of subclonal populations within the spheroid cultures the most plausible explanation. All of these patient-derived cultures appear polyclonal, highlighting the potential of using PDCOs to investigate tumor heterogeneity.

Phenotypic heterogeneity in patient-derived cancer organoids

In addition to molecular heterogeneity, phenotypic heterogeneity was identified within patient-derived cultures (Fig. 3). Within the same culture, type 1 (spheres with lumen) and type 2 (dense cellular spheres devoid of a lumen) organoids were commonly identified (27). These phenotypic differences were seen within samples across histologies (lung adenocarcinoma ML09, colon adenocarcinomas MC14 and DC46, and pancreatic adenocarcinoma DP41; Fig. 3A). It should be noted that on H&E from corresponding samples, the tumors were noted to be a mixture of well-differentiated areas composed of glands admixed with areas showing less gland formation with small clusters of cancer cells.

In addition to variations in sphere morphology, there were significant variations in the spheroid growth rate. Individual

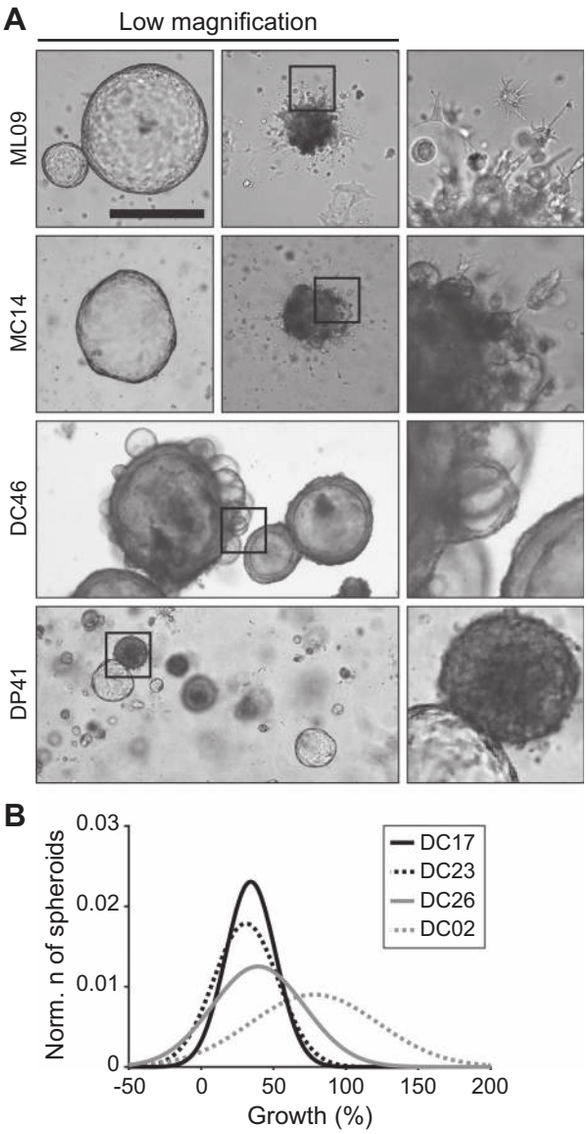

Figure 3.

Phenotypic heterogeneity exists within PDCOs (ML, lung adenocarcinoma; DC and MC, colorectal adenocarcinoma; DP, pancreatic adenocarcinoma). **A,** Across multiple cancers of different histology, both type 1 (spheres with lumen) and type 2 (spheres without a lumen) are observed within the same cultures. Scale bar for all low-magnification photos, 500 μm. Outlined areas are enlarged 4× in panels to the right. **B,** Population distribution modeling of growth of PDCOs over 48 hours.

PDCOs matured over 48–96 hours, and organoid diameter was measured at baseline and 48 hours later. Changes in the growth of individual spheres were plotted in population distribution histograms (Fig. 3B). Variation in the organoid growth rate was observed among cultures from different patients, and within the cultures from a given patient (Fig. 3B). Change-point analyses were performed to confirm that the growth rate of the organoids was not dependent on the baseline size for all PDCO lines. In addition, growth rate is independent of phenotype and location in the Matrigel.

Identification of differential response of colorectal cancer PDCOs to 5-FU chemotherapy and/or radiation

Chemotherapy and radiation are standard treatments for patients with locally advanced or metastatic colorectal cancer. We sought to resolve differential response among PDOCs treated with chemotherapy and radiation. PDCOs were generated from CRCs from five different patients. Spheroids matured in feeding media for 48–96 hours prior to treatment. Baseline brightfield images were acquired prior to treatment with 5-FU (0, 1, 10, or 100 μmol/L) and radiation (0, 2, or 5 Gy). The cells were exposed to 5-FU for 48 hours and radiation once. Brightfield imaging was performed again after 4 days. Change in diameter of individual organoids was measured and compared across samples and treatment conditions as a marker of response (Fig. 4A–E; Supplementary Fig. S1). A significant variation in the response to 5-FU and radiation was observed across samples. 5-FU and radiation were noneffective against DC17 with continued spheroid growth despite exposure to 100 μmol/L 5-FU and 5 Gy of radiation (Fig. 4A). This is in contrast to DC23, which was responsive to both 5-FU and radiation as evidenced by a significant reduction in median sphere size (Fig. 4B).

Population density modeling was then performed for those cultures treated with control, 10 μmol/L 5-FU, 2-Gy radiation, or the combination of radiation and 5-FU. Treatment response in this setting was defined by a shifting of the experimental curve to the left compared with the control curve and narrowing of the population (Fig. 4A–E, right column). Interestingly, population modeling identified potentially nonresponsive spheroid subpopulations. This is most evident in DC26, where the combination of 2-Gy radiation and 10 μmol/L 5-FU was exquisitely effective against part of the population, shifting the curve to the left, while an additional subpopulation remains unchanged compared with control (Fig. 4C).

To establish effectiveness thresholds, treatment effect sizes were calculated using Glass delta (22), which takes into consideration the treatment change as a function of the distribution of the control population. Glass delta was calculated for each treatment group (Fig. 4F). These values were then compared across the different patient samples and treatment conditions. The wide range of effect sizes (range, 0.07–3.39; Fig. 4F) highlights the differential response observed in these treatment studies. On the basis of these studies, and our prior experience with organotypic cancer spheroids, an effect size of 1.8 or greater was selected as the effectiveness threshold for diameter measurements in PDCOs. An effect size of greater than or equal to 1.5 and less than 1.8 indicates an intermediate response.

OMI measures PDCOs response to chemotherapy and radiation using cellular autofluorescence

Although changes in diameter can resolve differential treatment response, it is a limited metric that ignores cellular heterogeneity and underlying metabolic shifts that may precede changes in diameter. This is especially true for irradiated spheroids, which commonly shed cellular debris exterior to the spheroid wall, complicating diameter measurements. OMI was employed to refine the characterization of the PDCOs response to chemotherapy and radiation. This technique uses the inherent cellular autofluorescence of NAD(P)H and FAD to measure the metabolic activity of individual cells within spheroids without the use of dyes or disrupting the spheroid structure (28, 29). Previous studies have shown that OMI accurately predicts drug

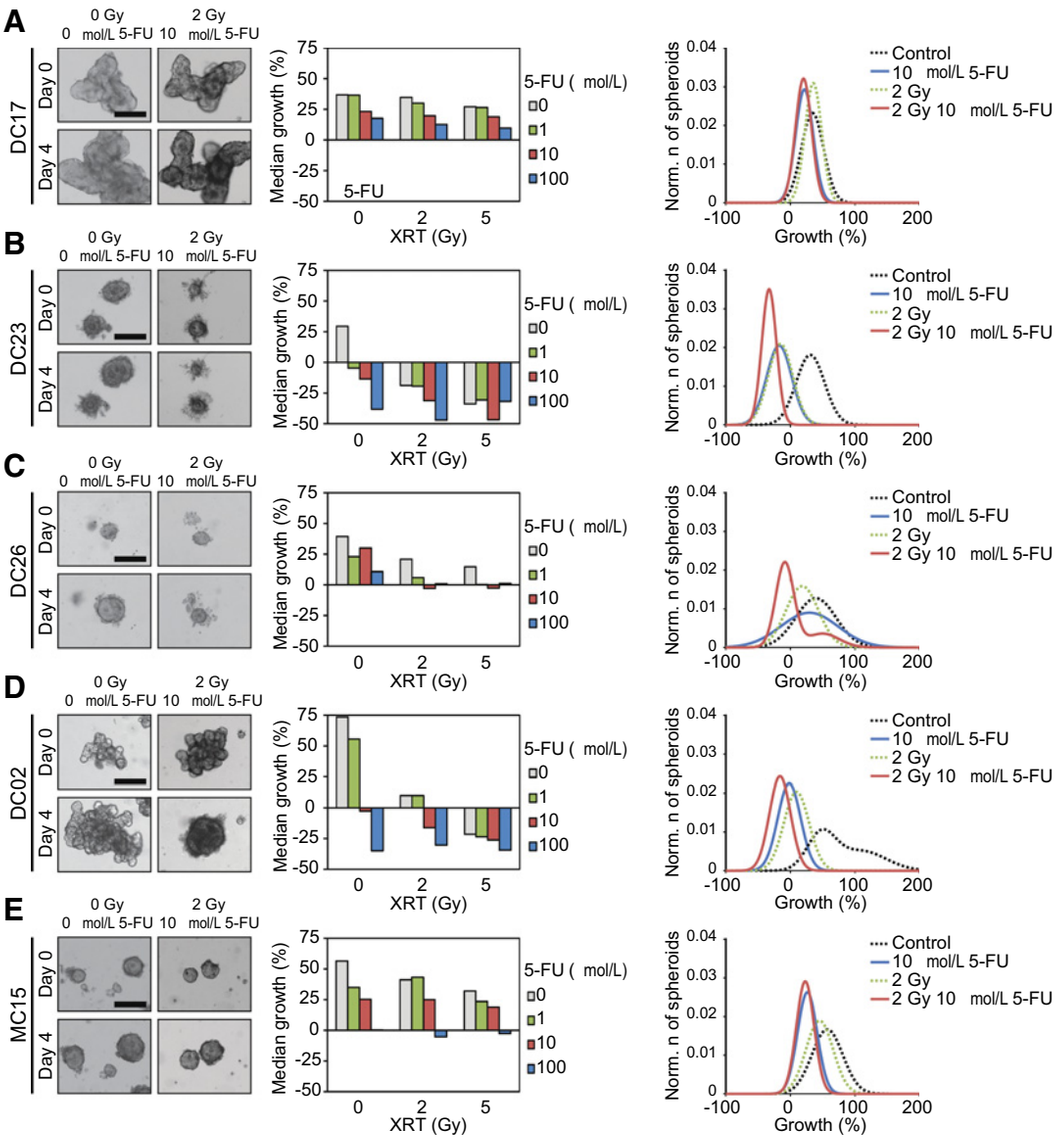

F

	DC17	DC23	DC26	DC02	MC15
0 Gy + 1 mol/L 5-FU	0.14	1.42	0.40	0.30	0.65
0 Gy + 10 mol/L 5-FU	0.73	2.16	0.31	1.81	1.27
0 Gy + 100 mol/L 5-FU	0.96	2.91	0.34	2.46	2.41
2 Gy + 0 mol/L 5-FU	0.07	2.07	0.66	1.55	0.49
2 Gy + 1 mol/L 5-FU	0.24	2.34	0.83	1.49	0.62
2 Gy + 10 mol/L 5-FU	0.81	2.86	1.09	2.13	1.41
2 Gy + 100 mol/L 5-FU	1.26	3.35	0.91	2.42	2.54
5 Gy + 0 mol/L 5-FU	0.31	2.74	0.94	2.17	0.96
5 Gy + 1 mol/L 5-FU	0.48	2.39	1.20	2.21	1.46
5 Gy + 10 mol/L 5-FU	0.87	3.39	1.23	2.34	1.72
5 Gy + 100 mol/L 5-FU	1.33	2.88	1.10	2.54	2.53

Figure 4.

Differential treatment response to chemotherapy and radiation treatment can be resolved using PDCOs. **A–E,** A total of five colorectal cancer PDCO lines were treated with increasing doses of 5-FU and/or radiation (0, 2, or 5 Gy) and then observed over 4 days. Brightfield images are for those PDCOs treated with control or 10 μmol/L 5-FU and 2-Gy radiation at baseline and 4 days posttreatment. Median spheroid growth (%) was measured for the different treatment conditions for each line. Growth is defined as change in spheroid diameter. Population distribution modeling was also performed to identify populations with different degrees of response to the treatments. Scale bars, 250 μm. **F,** Effect sizes, using Glass delta, were calculated for each treatment group across patient sample. Spheroid passage (p) numbers at the time of the treatment studies are: DC17 p2–3, DC23 p3-4, DC26 p1, DC02 p15-18, and MC15 11-12. Each treatment for each line was tested with 16–76 spheroids (median = 39).

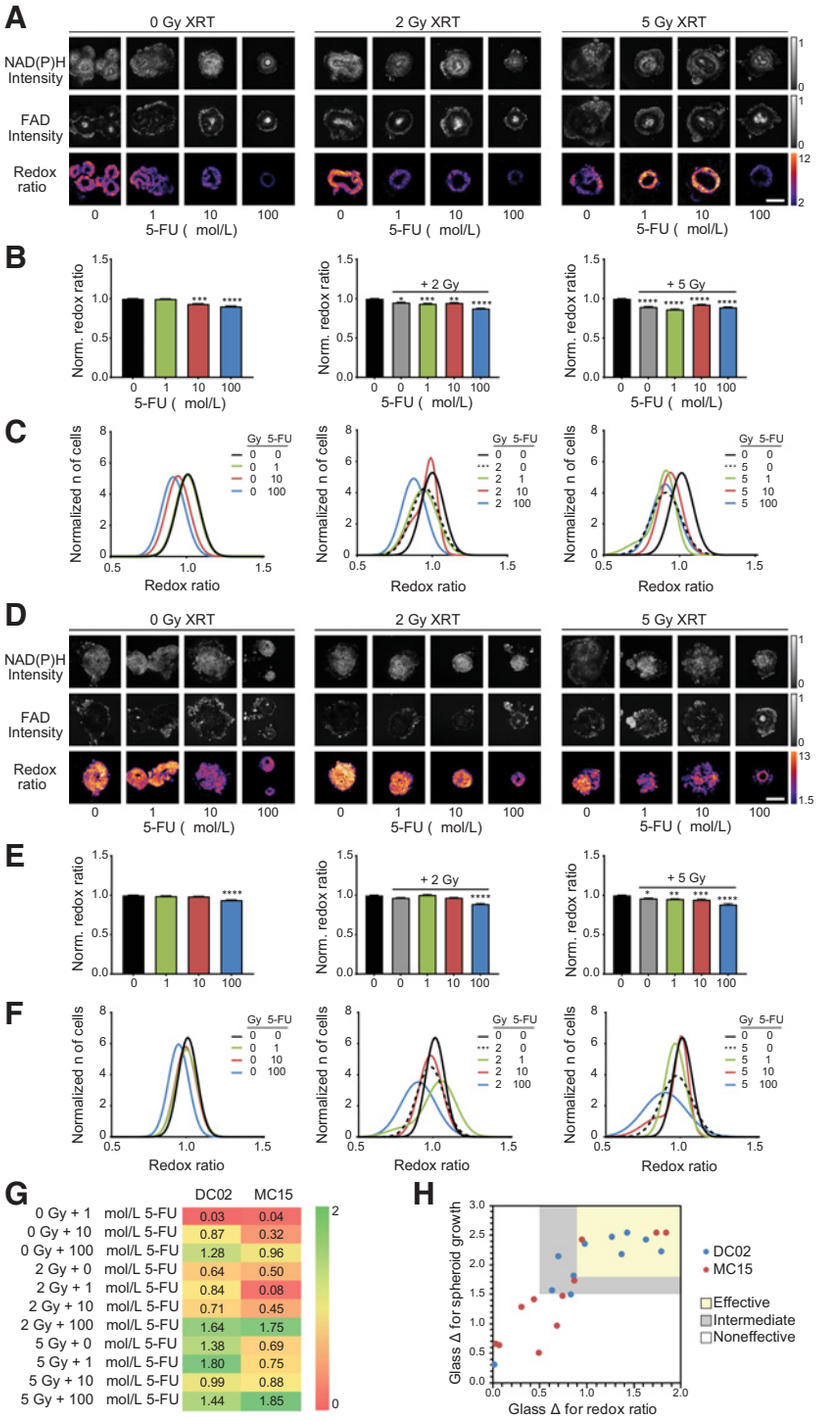

Figure 5.

DC02 (**A**–**C**) and MC15 (**D**–**F**). OMI of PDCOs 4 days post 5-FU and radiation. **A** and **D,** Images display the change in NAD(P)H and FAD intensity and the optical redox ratio across treatment groups. Scale bars, 100 μm. **B** and **E,** Normalized redox ratios are compared across treatment groups. **C** and **F,** Single-cell OMI analysis demonstrates the change in cell-level populations in response to 5-FU and radiation (cell number range 163–562). Asterisks represent effect size calculated from Glass delta. **G,** Heat map comparing the optical redox ratio effect sizes across treatment groups between DC02 and MC15. **H,** plot of the effect size (Glass delta) comparing the spheroid size and optical redox ratio analyses and using the combined measures to define treatment effectiveness. Each dot represents one treatment condition. *, Glass delta ≥ 0.6; **Glass delta ≥ 0.7; ***, Glass delta ≥ 0.8; ****, Glass delta ≥ 0.9. Spheroid passage (p) numbers at the time of the treatment studies are: DC02 p15-18 and MC15 11-12. Each treatment for each line was tested with 163–562 cells (median = 295).

effectiveness in patient-derived pancreatic and breast cancer spheroids, and human cell line–derived head and neck cancers (16, 18, 30–32).

OMI was performed alongside diameter measurements at the day 4 time point for two patient samples, DC02 (Fig. 5A–C; Supplementary Fig. S3) and MC15 (Fig. 5D–F; Supplementary Fig. S4). NAD(P)H and FAD intensities were measured and the redox ratio was calculated by dividing the NAD(P)H intensity image by the FAD intensity image. A reduction in the redox ratio was observed with increasing concentrations of 5-FU and increased radiation dose for DC02 (Fig. 5A and B). Glass delta was calculated for each treatment group to better approximate the effect size compared with control. These results indicate a high effect size after treatment with 100 μmol/L 5-FU alone, combined with 2-Gy radiation, and combined with 5-Gy radiation. The highest effect size was after 5-Gy radiation and subsequent 5-FU

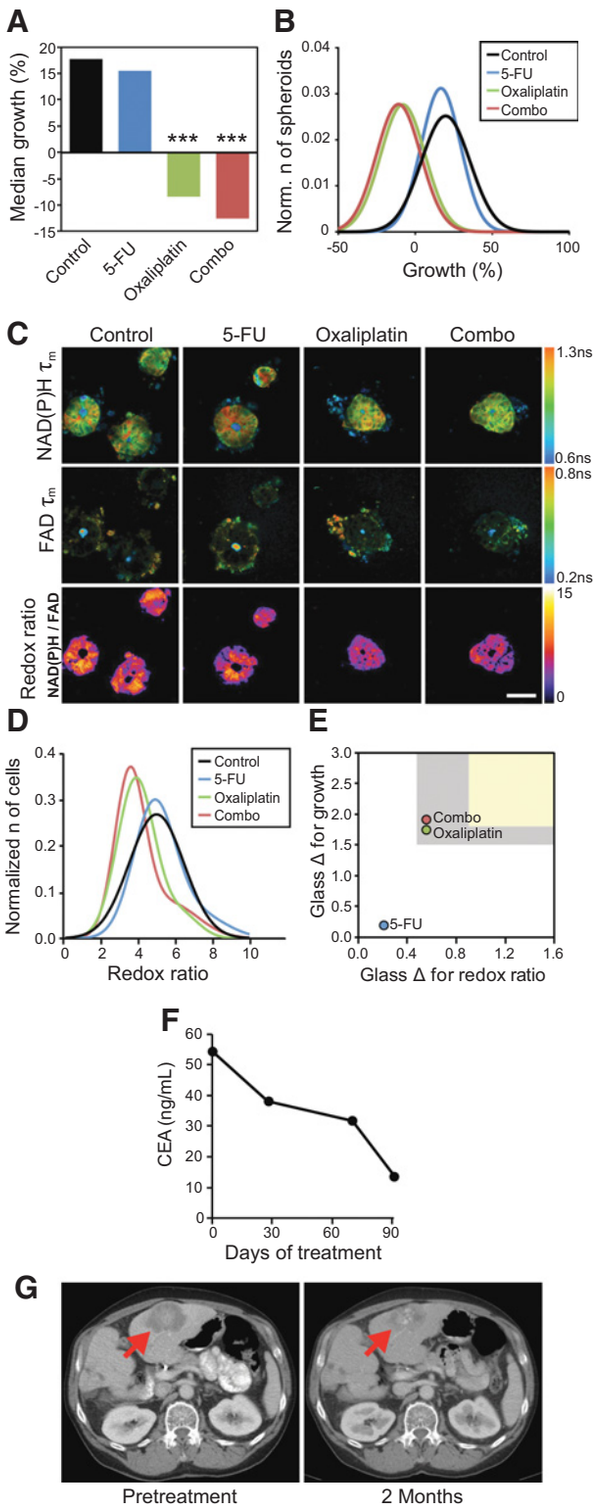

Figure 6.

PDCOs from a patient with treatment-refractory metastatic colorectal cancer (CRC) possessing alterations in *APC* and *TP53* were generated from a core needle biopsy of a liver metastasis. The subject had previously received 5-FU and oxaliplatin chemotherapy in the neoadjuvant setting approximately 4 years prior. Subsequently, the cancer had become resistant to a 5-FU–containing regimen. Clinically, there was the question of whether this patient could benefit from retreatment with 5-FU and oxaliplatin. **A,** PDCOs from this patient were treated for 48 hours with control, 5-FU (10 μmol/L), oxaliplatin (40 μmol/L), or the combination. A significant reduction in the median growth of the spheres was noted with the combination; however, lack of response was observed with the 5-FU treatment alone. ***, $P < 0.001$ (Wilcoxon rank-sum test). Growth is defined as change in spheroid diameter. Each treatment was tested with 64–98 spheroids. **B,** Population modeling based on spheroid size demonstrated a uniform lack of response to 5-FU and response to the combination of 5-FU and oxaliplatin. **C** and **D,** OMI confirms the lack of effectiveness of 5-FU for these PDCOs and response to the combination of 5-FU and oxaliplatin on a single-cell level. Each treatment was tested with 255–425 cells. Scale bar, 75 μm. **E,** Plot of effect sizes comparing the spheroid size and optical redox ratio analyses. **F,** Trend of the carcinoembryonic antigen (CEA) tumor marker in the response of this patient to 5-FU and oxaliplatin therapy. **G,** CT imaging of the subjects' liver metastasis before and 2 months after treatment with 5-FU and oxaliplatin. These studies were done on spheroids across passages 2–5.

treatments. These results are consistent with changes in spheroid diameter (Fig. 4). Further analysis with cell segmentation and population density modeling identified possible cell populations where this treatment was noneffective. A homogeneous treatment response (i.e., a unimodal distribution) was observed in the DC02 patient sample (Fig. 5C). MC15 was relatively nonresponsive to 5-FU and radiation with the most significant reductions in the redox ratio observed at the highest concentrations of 5-FU (Fig. 5D and E). Cell-level population analysis demonstrated uniform lack of response throughout the population, except with 2-Gy radiation in combination with 1 μmol/L 5-FU and 5 Gy radiation in combination with 10 μmol/L 5-FU where two populations with differing sensitivities could be resolved (Fig. 5F, middle).

The effect sizes were compared across patient samples and treatment groups (Fig. 5G). On the basis of these results and our prior experience, an effect size of 0.9 or greater was selected as the response threshold for the optical redox ratio, and an effect size greater than or equal to 0.5 and less than 0.9 was selected to represent an intermediate response. Next, we compared the diameter and optical redox ratio response assessments from the DC02 and MC15 experiments as both analyses were done simultaneously on these samples (Fig. 5H). There was general agreement across these analyses with 82% of treatments classified as either effective, intermediate, or noneffective by both analyses. There were four instances where there was a disagreement between the methods indicating a potential benefit for the combined analyses, especially for those samples falling in the intermediate range.

Prediction of effectiveness of therapies for a patient with metastatic colorectal cancer

PDCOs from a patient with treatment-refractory metastatic colorectal cancer possessing alterations in *APC* and *TP53* were generated from a core needle biopsy of a liver metastasis. The subject had previously received FOLFOX (5-FU, leucovorin, and oxaliplatin) chemotherapy in the neoadjuvant setting for metastatic disease approximately 4 years prior. The cancer progressed just 4 months after completing this regimen. Subsequently, the cancer became resistant to the 5-FU–containing regimen FOLFIRI and the EGFR inhibitor panitumumab. Clinically, there was the question of whether this patient could benefit from retreatment with FOLFOX chemotherapy. It has been published that a subset

of patients (~20%) previously treated with FOLFOX in the adjuvant setting will respond to this treatment if tried again (33). PDCOs from this patient were treated with 5-FU, oxaliplatin, the combination, or control (Fig. 6; Supplementary Fig. S4). Changes in spheroid diameter and redox ratios were analyzed. Lack of response to single-agent 5-FU was confirmed (effect size of 0.19 based on spheroid size and 0.21 based on optical redox ratio; Fig. 6A–E). Intermediate response of the PDCOs to the combination of 5-FU and oxaliplatin was observed on the basis of size and optical redox ratio effect size criteria (Fig. 6A–E) with an effect size of 1.92 for spheroid size and 0.56 for the optical redox ratio. The patient was subsequently retreated with FOLFOX chemotherapy. A reduction in the CEA tumor marker from 56 to 13 was observed over 3 months (Fig. 6F). A 10% decrease in cross-sectional diameter of the patient's liver lesion was found within two months of beginning the retreatment based on the RECIST version 1.1 response criteria (Fig. 6G; ref. 34). Continued therapy has maintained this response for more than a year.

Discussion

Advancements in 3D organoid cultures have enabled a better understanding of the biology of an individual patient's tumors in an efficient, cost-effective, and high-throughput manner. These cultures maintain the features of the cancers from which they were derived, including genetic alterations, metabolism, and drug response (11–17). For most cancer types, these cultures are rather pure populations of cancer cells and the tumor microenvironment is modeled using Matrigel and enriched culture media to represent some of the key factors produced by the tumor microenvironment. Our research group has demonstrated that organotypic spheroid cultures predict treatment response using multiple murine models (16–19, 28–32), indicating the need to further investigate spheroid cultures as a clinical tool.

Recently, Vlachogiannis and colleagues demonstrated that organotypic cultures derived from a small set of patients treated with a broad set of therapeutic agents could retrospectively predict response with an 88% positive predictive value and 100% negative predictive value using a generalized cell viability assay (12). In their approach, they utilized a more global measure of treatment response and did not investigate the heterogeneity within these cultures.

A major goal of this work was to gain further experience using PDCOs to predict effectiveness of chemotherapy and radiation for patients with cancer, including an improved understanding of the heterogeneity within these cultures. First, we demonstrate the ability to derive PDCOs from multiple different cancer types and confirm that these cultures are representative of the tumors from which they were derived in histology and molecular profile. Importantly, most of our cultures were generated with minimal supplementation to the media (Supplementary Table S2), which contrasts with the majority of published reports generating these cultures (11–17). To the best of our knowledge, this is the first description of PDCOs for the purpose of identifying differential responses in clinically relevant doses of both chemotherapy and radiation. Excitingly, we prospectively predicted response for a patient with metastatic colorectal cancer treated with retreatment FOLFOX chemotherapy. These analyses also demonstrated that this patient's cancer was nonresponsive to 5-FU alone, as was known clinically. Although this is exciting, clearly a larger experience is needed. This study in combination with prior analyses are major steps in that direction as these investigations allowed for the establishment of PDCOs treatment response thresholds using effect size measures to be further validated in larger prospective studies, which are now ongoing.

This study confirms the ability of PDCOs to characterize molecular and phenotypic heterogeneity and emphasizes the power of PDCOs to determine heterogeneity in therapeutic response. All of the organoids sequenced to date demonstrate the existence of subclonal populations, indicating that organotypic cultures could be a new tool to investigate evolution of the clonal architecture over time in response to therapies. Here we demonstrate that the molecular alterations found in PDCOs are highly representative of those seen within the adjacent tumor as also seen in prior investigations (11–17). The minor differences observed are comparable with the results of other studies sequencing different aspects of the same tumor (35). Notably, we observed substantial differences between spheroids and the adjacent tumor in a mismatch repair–deficient cancer. This is likely related to a higher degree of intrinsic heterogeneity in these cancers due to the increased mutation rate. It is also possible that clonal evolution continues within these cultures. Importantly, subclonal populations were resolved in these cultures. Future studies will examine the ability of these spheroid cultures to predict clonal evolution of a patient's cancer in response to anticancer treatments.

To further investigate heterogeneity within these cultures, OMI was used to interrogate the metabolic activity at the single-cell level. OMI exploits the intrinsic fluorescence of the metabolic coenzymes NAD(P)H and FAD to image therapeutic response across all cells in a 3D sample (28, 29). This single-cell analysis can dynamically quantify heterogeneous drug response, potentially identifying subpopulations where the treatment was noneffective (32). Importantly, OMI is performed through noninvasive interrogation of intact spheroid cultures to understand treatment response, heterogeneity, and mechanisms of resistance in the living, adapting spheroid. Therefore, OMI permits label-free interrogation over multiple time points.

On the basis of the findings here and the multiple prior studies cited above, the use of PDCOs to predict response for individual patients with cancer appears feasible. A combined measure using the change in spheroid size and change in the optical redox ratio appears to be a robust measure of response. This study is limited by its sample size, although it does establish effect size therapeutic thresholds. Future studies will validate these thresholds set in this manuscript. In addition, further studies will examine the use of PDCOs to quantify tumor heterogeneity and potentially predict the clonal evolution of the patient's cancer in response to therapies. Accurate prediction of treatment response is essential to improve individual patient outcomes. The organotypic culture and noninvasive assessment approach described here presents an exciting methodology to improve patient outcomes by avoiding unnecessary or toxic therapies for some patients while allowing for the escalation of therapies in responsive patients.

Disclosure of Potential Conflicts of Interest

M.F. Bassetti reports receiving commercial research grants from Merck, AstraZeneca, and EMD Serono. R.J. Kimple is an employee of International Journal of Radiation Oncology Biology and Physics; reports receiving commercial research grants from Ingynta and Peloton Therapeutics; and is a consultant/advisory board

member for Galera Therapeutics. No potential conflicts of interest were disclosed by the other authors.

Authors' Contributions

Conception and design: P.F. Favreau, M.F. Bassetti, D.A. Deming
Development of methodology: C.A. Pasch, P.F. Favreau, M.C. Skala, D.A. Deming
Acquisition of data (provided animals, acquired and managed patients, provided facilities, etc.): C.A. Pasch, P.F. Favreau, A.E. Yueh, C.P. Babiarz, A. Gillette, M.R. Karim, K.P. Nickel, A.K. DeZeeuw, C.M. Sprackling, R.A. DeStefanis, R.T. Pitera, S.N. Payne, D.P. Korkos, D. Miller, E. Carchman, M.E. Burkard, K.K. Lemmon, K.A. Matkowskyj, R.J. Kimple, D.A. Deming
Analysis and interpretation of data (e.g., statistical analysis, biostatistics, computational analysis): C.A. Pasch, P.F. Favreau, A.E. Yueh, C.P. Babiarz, A. Gillette, J.T. Sharick, A.K. DeZeeuw, C.M. Sprackling, P.B. Emmerich, R.T. Pitera, D.P. Korkos, L. Clipson, C.M. Walsh, D. Miller, K.A. Matkowskyj, M.A. Newton, I.M. Ong, R.J. Kimple, M.C. Skala, D.A. Deming
Writing, review, and/or revision of the manuscript: C.A. Pasch, P.F. Favreau, A.E. Yueh, A. Gillette, J.T. Sharick, P.B. Emmerich, S.N. Payne, L. Clipson, E. Carchman, M.E. Burkard, K.A. Matkowskyj, I.M. Ong, M.F. Bassetti, R.J. Kimple, M.C. Skala, D.A. Deming
Administrative, technical, or material support (i.e., reporting or organizing data, constructing databases): C.A. Pasch, D.P. Korkos, L. Clipson, K.K. Lemmon
Study supervision: M.C. Skala, D.A. Deming

Acknowledgments

The authors would like to thank the University of Wisconsin Carbone Cancer Center for the use of its Translation Science BioCore BioBank and Experimental Pathology shared service (supported in part by NIH/NCI P30 CA014520 to the UW Comprehensive Cancer Center Support) to complete this research. This project was supported by Funk Out Cancer, NIH P30 CA014520 (Core Grant, University of Wisconsin Carbone Cancer Center), UWCCC Experimental Therapeutics pilot award, Cathy Wingert Colorectal Cancer Research Fund, Wisconsin Partnership Program, Stand Up To Cancer (SU2C-AACR-IRG-08-16), Aly Wolff Foundation, NIH grants R37 CA226526, R01CA205101, R01CA185747, R01CA211082, the National Science Foundation CBET-1642287, start-up funds from the UW Carbone Cancer Center, UW Department of Medicine, UW School of Medicine and Public Health, the UW Graduate School through the Wisconsin Alumni Research Foundation, and the Morgridge Institute for Research. Stand Up To Cancer is a division of the Entertainment Industry Foundation. Research grants are administered by the American Association for Cancer Research, the scientific partner of SU2C.

The costs of publication of this article were defrayed in part by the payment of page charges. This article must therefore be hereby marked *advertisement* in accordance with 18 U.S.C. Section 1734 solely to indicate this fact.

Received November 9, 2018; revised March 8, 2019; accepted June 3, 2019; published first June 7, 2019.

References

1. Sholl LM, Aisner DL, Varella-Garcia M, Berry LD, Dias-Santagata D, Wistuba II, et al. Multi-institutional oncogenic driver mutation analysis in lung adenocarcinoma: the lung cancer mutation consortium experience. J Thorac Oncol 2015;10:768–77.
2. Solomon BJ, Mok T, Kim DW, Wu YL, Nakagawa K, Mekhail T, et al. First-line crizotinib versus chemotherapy in ALK-positive lung cancer. N Engl J Med 2014;371:2167–77.
3. Le DT, Uram JN, Wang H, Bartlett BR, Kemberling H, Eyring AD, et al. PD-1 blockade in tumors with mismatch-repair deficiency. N Engl J Med 2015; 372:2509–20.
4. Drilon A, Laetsch TW, Kummar S, DuBois SG, Lassen UN, Demetri GD, et al. Efficacy of larotrectinib in TRK fusion-positive cancers in adults and children. N Engl J Med 2018;378:731–9.
5. Fountzilas E, Tsimberidou AM. Overview of precision oncology trials: challenges and opportunities. Expert Rev Clin Pharmacol 2018;11: 797–804.
6. Naipal KA, Verkaik NS, Sanchez H, van Deurzen CH, den Bakker MA, Hoeijmakers JH, et al. Tumor slice culture system to assess drug response of primary breast cancer. BMC Cancer 2016;16:78.
7. Martinez NJ, Titus SA, Wagner AK, Simeonov A. High-throughput fluorescence imaging approaches for drug discovery using *in vitro* and *in vivo* three-dimensional models. Expert Opin Drug Discov 2015;10: 1347–61.
8. LaBarbera DV, Reid BG, Yoo BH. The multicellular tumor spheroid model for high-throughput cancer drug discovery. Expert Opin Drug Discov 2012; 7:819–30.
9. Schrag D, Garewal HS, Burstein HJ, Samson DJ, Von Hoff DD, Somerfield MR, et al. American Society of Clinical Oncology technology assessment: chemotherapy sensitivity and resistance assays. J Clin Oncol 2004;22: 3631–8.
10. Tentler JJ, Tan AC, Weekes CD, Jimeno A, Leong S, Pitts TM, et al. Patient-derived tumour xenografts as models for oncology drug development. Nat Rev Clin Oncol 2012;9:338–50.
11. van de Wetering M, Francies HE, Francis JM, Bounova G, Iorio F, Pronk A, et al. Prospective derivation of a living organoid biobank of colorectal cancer patients. Cell 2015;161:933–45.
12. Vlachogiannis G, Hedayat S, Vatsiou A, Jamin Y, Fernandez-Mateos J, Khan K, et al. Patient-derived organoids model treatment response of metastatic gastrointestinal cancers. Science 2018;359:920–6.
13. Dekkers JF, Berkers G, Kruisselbrink E, Vonk A, de Jonge HR, Janssens HM, et al. Characterizing responses to CFTR-modulating drugs using rectal organoids derived from subjects with cystic fibrosis. Sci Transl Med 2016;8:344ra84.
14. Matano M, Date S, Shimokawa M, Takano A, Fujii M, Ohta Y, et al. Modeling colorectal cancer using CRISPR-Cas9-mediated engineering of human intestinal organoids. Nat Med 2015;21:256–62.
15. Boj SF, Hwang CI, Baker LA, Chio II, Engle DD, Corbo V, et al. Organoid models of human and mouse ductal pancreatic cancer. Cell 2015;160: 324–38.
16. Shah AT, Diggins KE, Walsh AJ, Irish JM, Skala MC. In vivo autofluorescence imaging of tumor heterogeneity in response to treatment. Neoplasia 2015; 17:862–70.
17. Walsh AJ, Cook RS, Manning HC, Hicks DJ, Lafontant A, Arteaga CL, et al. Optical metabolic imaging identifies glycolytic levels, subtypes, and early-treatment response in breast cancer. Cancer Res 2013;73: 6164–74.
18. Walsh AJ, Skala MC. Optical metabolic imaging quantifies heterogeneous cell populations. Biomed Opt Express 2015;6:559–73.
19. Foley TM, Payne SN, Pasch CA, Yueh AE, Van De Hey DR, Korkos DP, et al. Dual PI3K/mTOR inhibition in colorectal cancers with APC and PIK3CA mutations. Mol Cancer Res 2017;15:317–27.
20. Pan W, Wall MM. Small-sample adjustments in using the sandwich variance estimator in generalized estimating equations. Stat Med 2002; 21:1429–41.
21. Akaike H. A new look at the statistical model identification. IEEE Transactions on Automatic Control 1974;19:713–23.
22. Glass GV, McGraw B, Smith ML. Meta-analysis in social research. London, United Kingdom: Sage; 1981.
23. Roerink SF, Sasaki N, Lee-Six H, Young MD, Alexandrov LB, Behjati S, et al. Intra-tumour diversification in colorectal cancer at the single-cell level. Nature 2018;556:457–62.
24. Weeber F, van de Wetering M, Hoogstraat M, Dijkstra KK, Krijgsman O, Kuilman T, et al. Preserved genetic diversity in organoids cultured from biopsies of human colorectal cancer metastases. Proc Natl Acad Sci U S A 2015;112:13308–11.
25. Pauli C, Hopkins BD, Prandi D, Shaw R, Fedrizzi T, Sboner A, et al. Personalized *in vitro* and *in vivo* cancer models to guide precision medicine. Cancer Discov 2017;7:462–77.
26. Sievers CK, Zou LS, Pickhardt PJ, Matkowskyj KA, Albrecht DM, Clipson L, et al. Subclonal diversity arises early even in small colorectal tumours and contributes to differential growth fates. Gut 2017;66: 2132–40.

27. Nagathihalli NS, Castellanos JA, Shi C, Beesetty Y, Reyzer ML, Caprioli R, et al. Signal transducer and activator of transcription 3, mediated remodeling of the tumor microenvironment results in enhanced tumor drug delivery in a mouse model of pancreatic cancer. Gastroenterology 2015;149:1932–43.
28. Skala MC, Riching KM, Bird DK, Gendron-Fitzpatrick A, Eickhoff J, Eliceiri KW, et al. *In vivo* multiphoton fluorescence lifetime imaging of protein-bound and free nicotinamide adenine dinucleotide in normal and pre-cancerous epithelia. J Biomed Opt 2007;12:024014.
29. Skala MC, Riching KM, Gendron-Fitzpatrick A, Eickhoff J, Eliceiri KW, White JG, et al. *In vivo* multiphoton microscopy of NADH and FAD redox states, fluorescence lifetimes, and cellular morphology in precancerous epithelia. Proc Natl Acad Sci U S A 2007;104:19494–9.
30. Walsh AJ, Cook RS, Sanders ME, Aurisicchio L, Ciliberto G, Arteaga CL, et al. Quantitative optical imaging of primary tumor organoid metabolism predicts drug response in breast cancer. Cancer Res 2014;74:5184–94.
31. Shah AT, Heaster TM, Skala MC. Metabolic imaging of head and neck cancer organoids. PLoS One 2017;12:e0170415.
32. Walsh AJ, Castellanos JA, Nagathihalli NS, Merchant NB, Skala MC. Optical imaging of drug-induced metabolism changes in murine and human pancreatic cancer organoids reveals heterogeneous drug response. Pancreas 2016;45:863–9.
33. Costa T, Nunez J, Felismino T, Boente L, Mello C. REOX: evaluation of the efficacy of retreatment with an oxaliplatin-containing regimen in metastatic colorectal cancer: a retrospective single-center study. Clin Colorectal Cancer 2017;16:316–23.
34. Eisenhauer EA, Therasse P, Bogaerts J, Schwartz LH, Sargent D, Ford R, et al. New response evaluation criteria in solid tumours: revised RECIST guideline (version 1.1). Eur J Cancer 2009;45:228–47.
35. Sottoriva A, Kang H, Ma Z, Graham TA, Salomon MP, Zhao J, et al. A big bang model of human colorectal tumor growth. Nat Genet 2015;47:209–16.